Recalibration of Eddy Viscosity Models for Numerical Simulation of Cavitating Flow Patterns in Low Pressure Nozzle Injectors

M. Coussirat[1]
LAMA,
Departamento Ingeniería Electromecánica,
Universidad Tecnológica Nacional,
C/Rodríguez 273,
Mendoza 5500, Argentina
e-mail: miguel.coussirat@frm.utn.edu.ar

F. Moll
LAMA, Departamento Ingeniería Electromecánica,
Universidad Tecnológica Nacional,
C/Rodríguez 273,
Mendoza 5500, Argentina

Cavitation in pressure injectors/atomizers affects the liquid/spray jet behavior at its outlet. The type of atomization induced by cavitation allows developing efficient devices if this cavitation state is controlled. Cavitating flow is related to turbulent and multiphase flows with mass transfer between the liquid and its gaseous phase and which is affected by several factors. Due to the high-speed flow and small spatial and time scales involved, the study of cavitating flows using physical experiments is very expensive. By means of numerical simulations using eddy viscosity models, some of the incipient and slight developed cavitating flow characteristics in nozzles are captured, but the level of the vapor fraction is commonly underestimated. It is evident that a suitable calibration of the turbulence models based on the special characteristics of the incipient/slight developed cavitating flows allows obtaining improved results. This special calibration is necessary due to the close relation between the cavitation inception/developing conditions and the turbulence level in the flow leading to a "nonstandard turbulence state." So, cavitating flows should not be modeled as a simple turbulent one. It is also demonstrated that the results obtained become competitive compared against the ones computed by large eddy simulations, which need a lot of computational resources and an appropriate initial solution for running. The conclusions obtained can be useful to improve injector designs because the suitable simulation of the incipient cavitation or slight developed cavitation flow conditions can be accurately simulated after calibration. [DOI: 10.1115/1.4049044]

Keywords: cavitation, turbulence, eddy viscosity models, validation/calibration, nozzle injectors

1 Introduction

The occurrence of cavitation inside a nozzle of a fuel injector for Diesel engines is directly connected with the local pressure drop. Cavitation is a complex phenomenon that appears in liquid flows when the local hydrodynamic pressure, p_c falls reaching the vapor pressure of the liquid, p_v. This low-pressure level provokes that the initial liquid flow becomes a two-phase flow, i.e., a mixture of liquid–vapor bubbles. The initiation of cavitation by liquid vaporization may require the existence of stresses lower than vapor pressure due to the surface stress tension in the bubble. However, the presence of undissolved gas particles, boundary layer effects, and turbulence fluctuations provokes changes in the values of this critical pressure p_c compared to p_v [1–3].

Computational fluid dynamics (CFD) codes based on a multiphase flow modeling technique, involving both mass transfer and turbulence submodels, have been specifically adapted/developed to study cavitating flows in the two last decades. For turbulence modeling, Reynolds-averaged simulation plus an eddy viscosity model (i.e., RAS + EVM) formulation for the mixture is now a common option for CFD simulations. For cavitating flow the transport equation-based modeling (TEM) is used, coupled with the RAS + EVM formulation [4–15]. The TEM models consist in solving a transport equation for either for mass or volume fraction with appropriate source terms to regulate the mass transfer between phases. These model combinations are frequently called RAS turbulent multiphase flow modeling (RAS/EVMs-TMF) [4–12].

Under this framework, this work is related to CFD modeling of cavitating flows in low pressure injectors having an asymmetrical nozzle inlet configuration and square sections at the outlet, see Fig. 1 [7–9]. The main subject here is to gain a deeper insight in the behavior and performance of specially calibrated RAS/EVMs-TMF models developed for general usage, when applied to design devices where cavitating flow appears into the nozzle. Previous works showed that a special calibration of the EVMs is necessary in cases of cavitating and confined flows and it must rely on physical evidence [10–12,16]. These calibration studies have been enhanced because more details about the physical framework involving the interaction between turbulence and cavitation have been considered to perform the calibration. So, some of the experiments used in the quoted works were revisited, and a revision of several works dealing with CFD applied to injectors was also made to improve the previous studies.

The calibration tasks consisted in a careful mesh sensitivity study and a suitable EVMs calibration parameters selection. This selection was performed considering the close relation between the cavitation inception/developing condition and the turbulence level in the flow considering the special characteristics of these detached flows.

Comparisons between the obtained results using calibrated EVM and large eddy simulations (LES) results from Refs. [7–9] were also made to check the quality of the solution offered by a

[1]Corresponding author.

Contributed by the Fluids Engineering Division of ASME for publication in the Journal of Fluids Engineering. Manuscript received March 26, 2020; final manuscript received October 30, 2020; published online December 11, 2020. Assoc. Editor: Daniel Livescu.

well calibrated EVM modeling, avoiding the intensive CPU requirements related to the LES simulations (i.e., very fine grids, small time steps, and an initial EVM solution to start the LES simulation).

After calibration, other goal was to check the possibility of detecting slight developed cavitation by obtaining some information related to the cavity shape and the outlet flow characteristics by means of a steady simulation using the ad hoc calibrated EVMs. The conclusions obtained here will be useful for subsequent CFD modeling of incipient, slight and fully developed cavitation states in nozzles with more complex geometries saving CPU resources compared with the ones needed for LES simulations.

2 Phenomenology of Cavitating Flows in Asymmetrical Nozzles

It is very important to understand the cavitating flow phenomenon into the injector nozzle, since it plays a significant role in its behavior (e.g., the fuel spray atomization), which strongly affects Diesel engine performances and emissions [7–9]. Several experimental and CFD databases for nozzles with symmetrical and asymmetrical inlet and different outlet sections exist, and a broad discussion and references related to the phenomenology of the cavitating flow in these nozzles can be seen in Refs. [7–9] and [17–19].

2.1 Experimental Data of Cavitating Flows in Asymmetrical Nozzles. Due to the high-speed flow and small spatial and time scales involved, the study of cavitating flows using physical experiments is very expensive although there are several experimental databases related to internal flow in injectors. Nurik's pioneering paper, used in several works related to calibration of codes in cases of cavitating flows in nozzles, was one of the firsts giving a clear evidence of the relationship between pressure variations into the cavity and its shape in cases of incipient and slight/fully developed cavitation (see full details and references in Refs. [11], [12], and [16]). More recently, detailed measurements of the mean velocity field and its turbulent fluctuations have been possible in cases of incipient or slight developed cavitation. These measurements, useful for CFD codes calibration, are now available; specifically, the databases related to low-pressure injectors from Refs. [7–9] are used in this work.

The experimental setup of Refs. [7–9] consisted in the use of a plunger pump to discharge filtered tap water at an ambient temperature (19 C) into ambient air through a rectangular nozzle, Fig. 1. The width, length, and thickness of the injector outlet (the nozzle) were $w_{out} = 1.98$ mm, $L_{out} = 8$ mm, and $th_{out} = 1.98$ mm, respectively. The width of the upstream region (injector inlet) is four times wider than the nozzle width. The liquid flow rate was measured using a flowmeter inserted in the hydraulic circuit. The static pressure upstream of the nozzle was measured, but the exact position of this pressure (gauge) probe was not clearly defined in

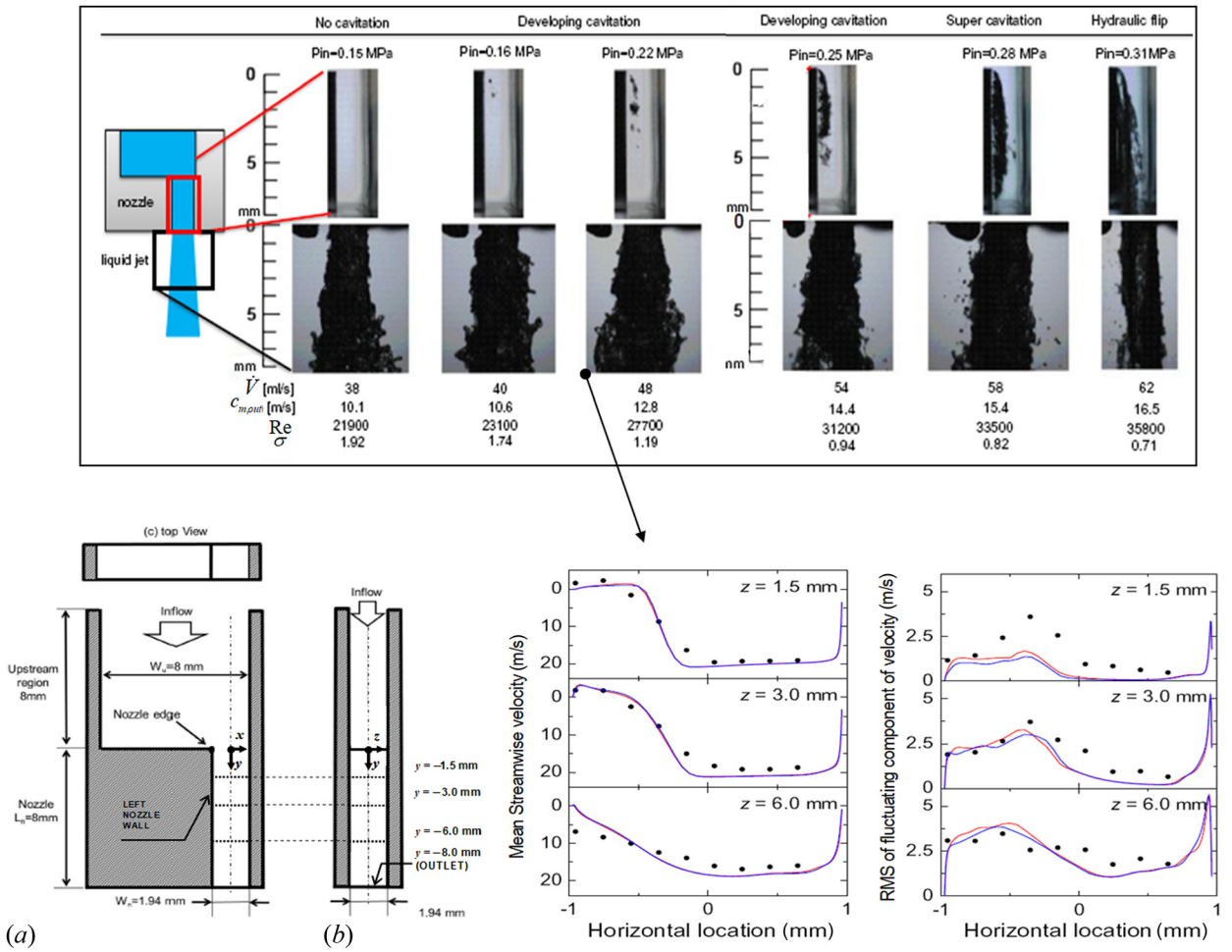

Fig. 1 Nozzle geometry, experimental cavitating flow patterns, mean velocity c_m and RMS velocity fluctuations, c'_{RMS} profiles, (for Re = 2.7×10^4) [7,9]. σ, Re-cavitation and Reynolds numbers, Eq. (1); p_{in}, inlet pressure; p_{out}, outlet pressure (=1.0×10^5Pa); p_v vapor pressure (=2.3×10^3Pa); ρ, liquid density (=998 kg/m^3); $c_{m,out}$, outlet mean velocity; w_{out}, nozzle width; ν, liquid viscosity (=1.35×10^{-6}m^2/s); •, Experiments (LDV); CFD from Ref. [7]: Smagorinsky (Red) and Vreman (Blue) LES SGS models, respectively. Note: For a clearer curves identification: Similar results were reported by the Smagorinsky and Vreman SGS LES models.

the experiments. In the x,y middle plane of the nozzle, Fig. 1 the mean streamwise velocity, c_m and its RMS fluctuation, c'_{RMS} profiles were measured using a laser Doppler velocimeter (LDV) system at three positions ($y_1 = -1.5$, $y_2 = -3.0$, $y_3 = -6.0$ mm). The uncertainties reported were –1% for the LDV and –3.7% for the flow rate measurements, respectively. Unfortunately, both the vapor fraction level and the local pressure values in the cavity were not reported.

Different cavitation states, from noncavitation to hydraulic flip (flipping flow), were reproduced, see Fig. 1. Commonly, these states are classified by characteristic numbers, i.e., Reynolds (Re) and Cavitation (σ) numbers, see Eq. (1), being: p_{inl}, inlet pressure; p_{out}, outlet pressure ($=1.0 \times 10^5$ Pa); p_v, vapor pressure ($=2.3 \times 10^3$ Pa); ρ, liquid density ($=9.98 \times 10^2$ kg/m^3); $c_{\mathrm{m,out}}$, outlet mean velocity; w_{out}, nozzle width; ν, liquid viscosity ($=1.35 \times 10^{-6}$ m^2/s); τ_s, surface superficial stress ($=7.28 \times 10^{-2}$ N/m)

$$\mathrm{Re} = c_{m,\mathrm{out}} w_{\mathrm{out}}/\nu \; ; \quad \sigma = (p_{\mathrm{out}} - p_v)/(0.5\rho\, c^2_{m,\mathrm{out}}); \qquad We = \rho c^2_{m,\mathrm{out}} w_{\mathrm{out}}/\tau_s \tag{1}$$

These states were generated changing the flow rate/inlet pressure, p_{inl}. The outlet pressure p_{out} remains constant and equal to atmospheric pressure because the nozzle outlet is a free subsonic jet. Negligible surface stresses influence is assumed by checking the Weber number (We), Eq. (1). This assumption is based taking into account that the We number is the ratio between inertial forces and forces due to surface stresses, being the surface stress effects not negligible only when We is ~O(1). A sensitivity analysis was performed changing both the density (computed using an assumed vapor fraction, *vf,* for the mixture of water and vapor) and the velocity (not necessarily the $c_{m,\mathrm{out}}$) values in the Eq. (1). Taking representative values for the vapor fraction at incipient cavitation state (e.g., $vf = 0.75$) and $c_{m,\mathrm{out}}$ of O(1), the computed We is ~O(10), meaning that under these "extreme" conditions the inertial stresses are almost ten times bigger than the surface stresses. At this incipient cavitation state, the assumed vapor fraction level could be representative of a typical very small cavity with a size of ~O($0.1w_{\mathrm{out}}$), placed downstream the nozzle edge, see Fig. 1. This fact could justify with certain confidence the assumption of negligible surface effects under this cavitation state because the cavity has a very local effect on the flow structure being more important the detachment effect after the nozzle edge, see Fig. 1.

Depending on the cavitation state generated, different visualization techniques were used for the cavity observation. For noncavitation and incipient cavitation conditions, still images of cavitation and a liquid jet were taken by using a digital camera (3008×2000 pixels) and a flash lamp (pulse duration = 4 μs). For the full developed cavitation state, the cavity evolution was captured using a high-speed camera (frame rate = 20,000 fps, exposure time = 50 μs) and a reflector lamp.

Notice that Re-and σ numbers are not closely related, and both are necessary for the flow classification [7,11,12]. For certain p_{out} and p_v values already defined, the σ value goes down when the flow rate is increased. Into the range $1.74 < \sigma < 1.19$, the flow separation occurs only at the sharp-edged inlet of the nozzle, and the incipient cavitation condition appears only along the left nozzle wall in the zones nearer the nozzle inlet. A huge number of bubble nuclei starts growing for lower σ values and vortices appear downstream the detachment point in the low-pressure zones within the recirculation region, i.e., the developed cavitation state starts, Fig. 1.

Strong decrements in the σ values provoke that the vortices appear clearly and then, they are advected downstream. They are also accompanied by clouds of vapor bubbles that collapse during the shedding when the pressure rises downstream again, i.e., the transition from developed cavitation to supercavitation states takes place. It can be observed that this transition has a quite unsteady behavior, probably due to the short length of the nozzle in this case (i.e., a ratio $L/w < 5$), being this fact an additional difficulty for the CFD modeling [11,12].

2.2 Useful Conclusions From Previous Computational Dynamic Fluids Results for Cavitating Flows. The dependence between turbulence and cavitation models has been extensively investigated, see selectively the works from Refs. [5–9], [11], [12], [16], and [20–24]. In the results obtained for the incipient cavitation state, it was demonstrated that there is a higher dependence on the turbulence models than on the cavitation models selected [8,9,11,12,16]. The cavitation models checked [13,14,25] have shown slight differences in the cavity shape and vapor fractions levels predicted.

One of the goals here is to enhance the investigation from previous works [11,12,16], which were focused in the EVMs calibration because it becomes clear that there is a close relation between the cavitation inception/developed condition and the turbulence level in the flow. The spatial distribution and the decay rate of the turbulence level produced by cavitation could be related to some preferred turbulence scales present in the process, which lead to a "nonstandard turbulence state." So cavitating flows should not be modeled as typical turbulence. Usually, uncalibrated EVMs overpredict the μ_t level in cavitating nozzles/Venturi flows [11,15]. This fact leads to compute lower values for the dynamic pressure yielding a higher absolute pressure value and less cavitation. The μ_t overestimation affects directly the cavitation region due to the high stresses computed and limits both the level of the vapor fraction and the velocity distribution in the recirculation zones.

Other goal of this work is to compare EVMs results against the ones obtained by LES because it is known that LES modeling allows obtaining a more detailed cavity shape in cases of slight developed cavitation, what requires higher computational (CPU) resources. In order to give an answer to the question whether it is possible to obtain enough resolution in the flow pattern and the cavity shape at an inception or slight developed cavitation state by using EVMs, some CFD works related to LES simulations were used for comparisons [7,9].

The referred works presented CFD results involving RAS and LES simulations in the same asymmetrical nozzle configuration, Fig. 1. Two subgrid scale (SGS) submodels (Smagorinsky and Vreman, respectively) were selected for LES modeling, joined to the Lagrangian bubble tracking method and to the modified Rayleigh (MR) Plesset equation model. Some comparisons against RAS/EVM simulations were also carried out by these authors who investigated three EVM turbulence models (standard k–ε, shear stress transport (SST) k–ω, renormalization group (RNG) k–ε) combined with the MR model. It is highlighted that Ref. [9] uses the standard wall functions for the standard k–ε and the RNG k–ε models, but for LES simulations, the Van Driest damping was used. They concluded that the results obtained by LES under the incipient cavitation condition (σ – 1.19) gave a good prediction for the cavity length, its thickness, and the incipient cavitation cloud shedding. However, an LES simulation required a very fine grid, small time steps, an initial solution to start the LES simulation and high CPU resources [7,9]. On the other hand, the combination MR/RNG k–ε models gave a good prediction for the cavitation length and thickness using a locally refined grid with a minimum length cell of h–50 μm = 0.05 mm for an outlet of wide, $w_{\mathrm{out}} = 2.0$ mm and using less CPU resources than the LES simulation. The incipient cloud shedding was well reproduced by both the MR/RNG k–ε and the MR/SST k–ω models by using a grid with a length cell into the range $25\ \mu\mathrm{m} < h < 50\ \mu\mathrm{m}$ and time steps of O(10^{-8}s). Seemingly, in cases of developed cavitation, the cloud shedding was only qualitatively well simulated by these EVMs because there is not any comparison for the shedding frequencies. Both the recirculation flow and the vortex shedding accompanied by cavitation clouds until the nozzle outlet were captured only with the combination of the MR/LES models using a fine grid having a minimum grid cell size of h~4.4 μm. The

study concluded that the MR equation model combined with an appropriate turbulence model (EVMs or LES) and using a very fine grid can simulate the complex cavitating recirculation flow, the cloud cavitation shedding, and the reentrant jet flow. This combination can simulate quantitatively the cavitation thickness, the cavity length, the mean, and the fluctuating turbulence velocities too. The main problem remains in the high CPU requirement for these steady/unsteady simulations due to the refined grids and short time steps necessary [7,9,22].

3 Defined Methodology for Calibration

The previous discussion allows defining the present methodology. The main goal here is to check the possibility of detecting incipient cavitation by obtaining some information related to the cavity shape and the outlet flow characteristics by means of a steady state simulation using ad hoc calibrated EVMs. The conclusions obtained here will be useful for subsequent CFD modeling of incipient, slight, and fully developed cavitation states in nozzles with more complex geometries saving CPU resources.

The following methodology was defined, namely, (1) to perform a detailed "grid independence study" in the obtained results, using the grid convergence index (GCI) combined with the Richardson extrapolation techniques [26–30] for a noncavitation/incipient cavitation state, i.e., $\sigma = 1.91$. (2) To perform a detailed EVMs calibration using some of the previous results obtained in Refs. [11,12,16] for a developing cavitating flow ($\sigma = 1.19$).

It is known that unsteady simulations of cavitating flows are expensive and time-consuming [8,9,21–23]. Related to the possibility of steady-state simulations, the work from Vashahi et al. [23] pointed out the difficulty encountered in the simulations of cavitating flow by steady-state simulations using EVMs. Unfortunately, the cavitation state studied (i.e., incipient, slight developed, fully developed) is not clearly reported in this work; therefore their conclusions concerning to the difficulties to perform steady simulations due this fact they are not unquestionable.

However, in this work, the possibility of steady flow CFD simulations was checked by means of computing the Strouhal number, $\mathrm{Sr} = L_\sigma (c_\sigma\ t)^{-1}$ being L_σ, t and c_σ the characteristic unsteadiness scales for length, time and velocity, respectively. In order to define suitable values for these scales, the conclusions presented in Refs. [12] and [31] were taken into account leading to define the following values for the variables at the incipient cavitation state ($\sigma = 1.19$), i.e., $L_\sigma \sim w_{\mathrm{out}} = 1.98$ mm, $t = 0.01$ s and $c_\sigma = c_{m,\mathrm{out}}\sqrt{1+\sigma} = 18.9$ m/s. The value for the Strouhal computed is $\mathrm{Sr} = 0.01$ and the selected cases could look like a steady phenomenon correlated to the low shedding frequencies under an incipient cavitation state, i.e., O(25-250 Hz) [31,32].

3.1 Turbulence and Cavitation Models Selected. Four EVM turbulence models, i.e., the Spalart Allmaras (SA), the standard k–ε (Ske), the shear stress transport (SST) k–ω, and the renormalization group (RNG) k–ε were used. Full details and references for all the EVMs used can be seen in Refs. [33–36], and [37]. A previous estimation of the cell size needed in the used grid, based on a value of $y+ = 15$ was made to avoid the use of wall functions in the selected EVMs that require this strategy because the flow into the nozzle is not developed (i.e., there is no autosimilarity in the velocity profiles along the nozzle). Then, when a grid convergence study is performed, the use of the wall-function approach could fail if this approach is used in inappropriate zones near the wall. For the cavitation modeling, the TEM model from Singhal et al. [13] was selected because this model showed good performance in previous works [11,12,16].

3.2 Geometry, Boundary Conditions, and Discretization Schemes Defined. A commercial CFD code [38] was used for the simulations on the selected geometry, Fig. 1. Five conformal and homogeneous successively refined grids with a cell area of $h \times h$, were built, see Table 1. The inlet boundary condition was defined as a mean value for the velocity, which was computed from the mass conservation principle because the geometry sections at the inlet and outlet, and the nozzle outlet velocity for each case are known in advance. The turbulence boundary conditions were computed from standard formulations for each EVM [33,38]. At the outlet, a defined pressure value was imposed ($=1.0 \times 10^5$ Pa) and a nonslip condition was defined at the walls. The selected discretization schemes were: QUICK for density, vapor fraction, momentum equations and turbulent quantities, PRESTO for pressure, and SIMPLEC for pressure–velocity coupling, see details in Refs. [33] and [38]. After the CFD modeling, the predicted inlet pressure p_{in} and its corresponding σ value were verified for each case, see Fig. 1.

3.3 Grid Sensitivity Study. It is very important to know what kind of information is needed in a CFD study because different parameters will converge differently. When a higher order parameter is being computed/predicted, such as the local wall friction, the grid requirements might be stricter than the ones required for an integral quantity (i.e., lower order parameters) such as mean pressure, mean velocity, or drag coefficient. If it is necessary to analyze both high and low order properties in a simulation, then a very rigorous grid convergence study of primitive, integrated, and derived variables is mandatory [22,26–30].

Considering much advice concerning the turbulent flow modeling in confined flows from Roache [28], the GCI method combined with the Richardson extrapolation was applied to check the uncertainty in the selected variables. Initial simulations for a noncavitating flow state ($\sigma = 1.91$, Fig. 1) were carried out by using five successively refined grids. This GCI+Richardson extrapolation study was performed for the SA, the Ske and the SST models to have guarantee of the grid independence in the computed results. For the CGI analysis, three sets of grids were defined. Each one comprises three consecutively refined grids (i.e., sets M05-03, M04-02, M03-01, see Table 1).

In order to verify the local $y+$ values previously computed by hand, a preliminary CFD simulation was performed using the SA model because it is simpler and it automatically switches its formulation for high or low Reynolds flow conditions. The GCI+Richardson extrapolation study was performed considering that the grids used must fulfill the condition $3 < y^+ < 15$ to obtain an accurate near wall modeling. The use of finer grids requires the low Reynolds correction usage for the SST model and high CPU resources for all EVMs. Otherwise, the use of coarser grids implies an inadequate wall-function usage for the RNG and Ske models in this kind of nondeveloped flows [33,34,38].

Global mass conservation was checked in all the simulated cases by computing the relative difference between the inlet/outlet mass flows. The GCI+Richardson extrapolation study was carried out for the following parameters, namely, ϕ_1, mean pressure at position y_3; ϕ_2 mean velocity c_m, at position y_3; ϕ_3 outlet mean velocity $c_{m,\mathrm{out}}$, (related to the outlet flow rate) and ϕ_4 an ad hoc defined parameter, y^+_m Eq. (2) (i.e., an "averaged" Re-along the left nozzle wall, Fig. 1)

$$y_m^+ = \varphi_4 = \frac{1}{N_h}\sum_{i=1}^{N_h}\left[x_i\sqrt{\tau_{w,i}/\rho}/\nu\right] \tag{2}$$

Table 1 Grids and set of grids defined: set M05-03 has M05, M04, and M03 grids

	M05	M04	M04(3D)	M03	M02	M01
h (mm)	0.16	0.08	0.08	0.04	0.02	0.01
Cells (Adim)	3,600	12,300	326,400	50,000	198,800	795,200
y^+_m (Adim)	13.27	12.40	11.63	5.91	3.02	1.53

Sets M04-02 and M03-01 have been defined in a similar way. h: cells side and y^+_m: averaged local Re-along the left nozzle wall, Eq. (2).

Being ρ, ν, the density and the viscosity of the liquid phase, respectively; N_h, the number of cells along of the left nozzle wall; x_i, the distance from this wall to each cell center and $\tau_{w,i}$, the local wall stress in each cell. The results obtained for ϕ_3 can be seen in Fig. 2, where the h values in the graphics in Fig. 2 are the corresponding cell length for each grid. The log–log figures highlight the difficulties in the choice of the mesh cell size because the number of cells is greatly increased when h goes down, see Table 1. The cells size of each mesh is showed in Fig. 3 for comparisons.

It is remarked that the asymptotic value computed by the Richardson's extrapolation (i.e., for $h \to 0$) for all the variables ϕ_i shows some variations, depending on the set of grids used for the asymptotic value computation in each case (i.e., M05-03, M04-02, M03-01).

For all the EVMs used, the asymptotic range was reached for the ϕ_1, ϕ_2, and ϕ_3 in the sets M05-03 and M04-02. Instead, ϕ_1 does not reach the asymptotic range when the Ske is used in the set M03-01. The variable ϕ_4 never reaches the asymptotic range because it is closely related to the grid size defined (a nonasymptotic value). The ϕ_2, ϕ_3, and ϕ_4 variables showed a monotonic convergence, but the variable ϕ_1 showed an oscillatory convergence depending on the EVM used for the M04-02 and M03-01 sets.

Concerning to the observed asymptotic behavior of ϕ_1, this fact could be correlated with the difference in the order of the mass conservation residuals obtained. When the M05-M02 grids were used, the difference was of $O(10^{-6})$, but the flow rate difference only reached an $O(10^{-4})$ for the grid M01. The computed pressure field showed some instability near the nozzle inlet for the M01 grid too. These oscillation levels were of 5–7% around the mean value computed of $O(\pm 10^{4})$ for the pressure at position y_3, a phenomenon not observed in the M05-M02 grids. It is highlighted that cavitating flow is related to the p_v with a value of order $O(10^{+3})$. Then, the observed pressure instability computed for all EVM used could provoke an artificial incipient shedding, even though the experiments do not show any clear cavitating flow pattern. This artificial shedding, affecting the order of convergence in the mass flow, could be related to the near-wall modeling (NWM) strategy involved for the M01 grid, implying a more accurate low-Renumber modeling strategy (e.g., well calibrated damping functions). It is highlighted that depending on the EVM used, the NWM is automatically activated/switched by the CFD code [38].

Hence, these levels of variations in the predicted pressure ϕ_1 could be responsible for the predicted cavitation state, being the pressure a variable more sensitive than the velocity to the NWM strategy selected [11,27]. Here, the correlation between pressure fluctuations and turbulence could play a role of paramount importance and further research would be necessary to explain the relation between the NWM strategy selected/used and the behavior in the asymptotic range for ϕ_1. Unfortunately, there are no ϕ_1 experimental values for a comparison, adding difficulty to perform/enhance the EVMs calibration tasks.

Despite these difficulties, the GCI check performed allows to state with some confidence that grids M03 and M04 have enough resolution and fulfill the $y+$ requirements for the subsequent EVMs calibration task.

Likewise, to check the influence of the two-dimensional flow assumption two- and three-dimensional cases (called 2D and 3D, respectively) were compared for the M04 grid, extending this 2D grid by its extrusion to a 3D case. The results obtained for these grids showed slight differences when the 3D case (at its xz middle plane) and the 2D case were compared. In the 3D case, the symmetry fulfillment of the results obtained for both the velocity and pressure fields along the yz middle plane was also checked. The major drawback for the 3D solution is a mass conservation of only an error of $O(10^{-4})$ against the $O(10^{-6})$ observed in the 2D case for the SA model. Despite this drawback, some 3D effects were observed confined only at the corner among the top/bottom walls and the sharp-edged nozzle inlet, but they do not affect the general flow pattern.

Therefore, it was verified that there are negligible differences between the obtained 2D and the 3D results. As a result, a similar behavior for 2D/3D cases for the M03 grid should be expected. Then, subsequent 2D simulations for the developing (incipient) cavitation state (i.e., $\sigma = 1.19$) will be performed for the EVMs checking/calibration.

3.4 Detailed analysis of the Shear Stress Transport k–ω Model for Its Calibration. Previous works from the authors [11,12,16] showed that it is possible to improve the obtained results for cavitating flows in nozzles by means of careful EVM calibration. After its good behavior during the already mesh sensitivity study, the SST model [35,39] was selected here foreseeing its applications for unsteady state turbulent cavitating flow modeling by using a modified version of it, including the called scale-adaptative simulation (SAS) strategy [40,41].

The SST model is a two-equation turbulence model, Eqs. (5) and (6) where the kinematic turbulent viscosity $\nu_{t,m}$ is computed by means of a combination of two variables representing turbulence scales: the turbulent kinetic energy k, and its rate of dissipation ω, Eq. (3). These variables selected to compute $\nu_{t,m}$ are based on the dimensional analysis theory and computed by a transport equation of each one, Eqs. (4) and (5).

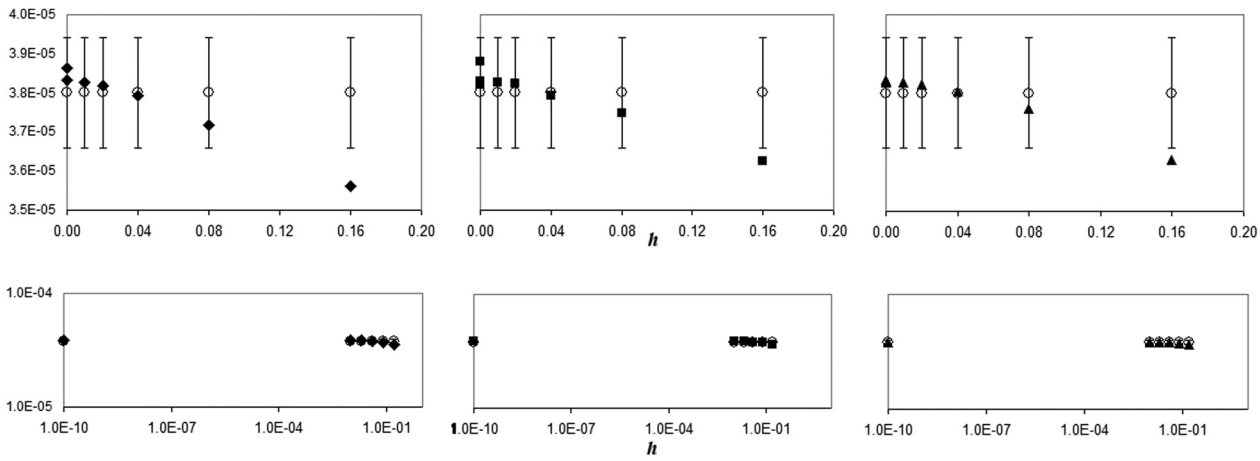

Fig. 2 GCI study: Outlet flow rate (m^3/s) computed versus cell size h (mm), experiments from Refs. [7] and [9]. Top: linear scale, bottom: log–log scale (x-axis value 1.0×10^{-10} means "tending to zero"). ○, Exp. (vertical bars point out the experimental uncertainty):◆, Ske; ■, SST;▲,SA.

The two terms on the left-hand side of the transport equations, Eqs. (4) and (5), are, respectively, the local and the convective variation of the variable (k or ω). The four terms on the right-hand side of the equations are, respectively: production, diffusion, dissipation, and source for the variable (k or ω). In the Eq. (5) the last term, $D_{\omega,}$ is the damped cross-diffusion derivative term.

It is highlighted that the SST model is based on the blending between the standard k–ω and the standard k–ε (Ske) models. To blend these two models together, the Ske model has been transformed into equations based on k and ω, which leads to the introduction of the aforementioned D_ω term

$$\nu_{t,m}=\frac{1}{\max\left(\frac{1}{\alpha^*},\frac{SF_2}{a_1\omega}\right)}\left(\frac{k}{\omega}\right);\omega=\varepsilon k^{-1};S_{ij}=\frac{1}{2}\left(\frac{\partial u_j}{\partial x_i}+\frac{\partial u_i}{\partial x_j}\right);S=\left|\sqrt{S_{ij}S_{ij}}\right| \tag{3}$$

$$\frac{\partial k}{\partial t}+u_i\frac{\partial k}{\partial x_i}=\min\left(2\nu_t S_{ij}S_{ji};10\beta^* k\omega\right)+\frac{\partial}{\partial x_i}\left[\left(\frac{\nu_T}{\sigma_k}+\nu\right)\frac{\partial k}{\partial x_i}\right]-\beta^* k\omega+S_k \tag{4}$$

$$\frac{\partial \omega}{\partial t}+u_i\frac{\partial \omega}{\partial x_i}=\alpha\alpha^*\left(\frac{\omega}{k}\right)2\nu_t S_{ij}S_{ji}+\frac{\partial}{\partial x_i}\left[\left(\frac{\nu_T}{\sigma_\omega}+\nu\right)\frac{\partial \omega}{\partial x_i}\right]-\beta\,\omega^2+S_\omega+D_\omega \tag{5}$$

$$\begin{aligned}
\alpha^* &= f_1(\alpha^*_\infty,\alpha^*_0,\mathrm{Re}_t,R_k);\ \mathrm{Re}_t=\rho k(\mu\omega)^{-1};\\
\beta^* &= f_2(\beta^*_\infty,\mathrm{Re}_t,\mathrm{Re}_\beta)\\
\alpha &= f_3(\alpha_\infty,\alpha_0,\mathrm{Re}_t,R_\omega);\ \alpha^*_0=f_4(\beta_i);\beta=f_5(\beta_i)\\
\alpha_\infty &= f_6(\alpha_{\infty,\mathrm{inner}},\alpha_{\infty,\mathrm{outer}},F_1,F_2)\\
\alpha_{\infty,\mathrm{inner}},\alpha_{\infty,\mathrm{outer}} &= f(\beta^*_\infty,\kappa,\beta_{\mathrm{i,inner}},\beta_{i,\mathrm{outer}},\sigma_{\omega,\mathrm{inner}},\sigma_{\omega,\mathrm{outer}})\\
\beta_i &= f_8(\beta_{i,\mathrm{inner}},\beta_{i,\mathrm{outer}},F_1,F_2)
\end{aligned} \tag{6}$$

Finally, $\kappa, \sigma_{\mathrm{k,inner}}, \sigma_{k,\mathrm{outer}}, \sigma_{\omega,\mathrm{inner}}, \sigma_{\omega,\mathrm{outer}}, \alpha^*_\infty, \beta_{\mathrm{i,inner}}, \beta_{\mathrm{i,outer}}, \alpha_0, R_k, R_\beta, R_\omega, \beta^*_\infty, a_1$, are parameters for calibration and F_1, F_2 are blending functions that "connect" the high and low Re number zones in the boundary layer. After the observation of these equations, it is clear that the calibration of the SST model for a CFD user who does not know the full details of the model is not easy, due to the fact that there are many parameters to perform this task and there is not a clear information related to the role of each one of these parameters plays.

At this stage, it would be interesting to know which ones are more relevant for a fine-tuning in modeling tasks related to cavitating flows in nozzles, since the obtained CFD results could be improved if a suitable control of the $\mu_{t,m}$ level is obtained by some kind of special calibration. Previous works give some ideas related to this fact [10–12,15,16,36]. A possible improvement could be obtained by performing an analysis that allows identifying which of them has more influence in the computed level of $\nu_{t,m}$. It is necessary to take into account that by ensuring low levels of $\nu_{t,m}$ in zones of low pressure could lead to a suitable prediction of the cavitation inception because predictions of nonrealistic high levels of $\nu_{t,m}$ dampen out the unsteady flow structures [10,15]. Spalart et al. [36] suggested that in cases of anisotropic turbulent flows, the computed level of $\nu_{t,m}$ can increase only by modifying the effects of its production.

Following these ideas, and as a result of the analysis performed in previous calibration studies [11,12,16], the parameter β^*_∞ was selected for calibration, since it is responsible for the computed level in the dissipation of k, and the production of ω (Eqs. (4)–(6)) and also controls the boundary conditions computed for k and ω at the walls [11,12,16,35,37,39]. The base value for β^*_∞ (=0.09) has been established by examining the so-called wall layer [42]. In boundary layer flows, the wall layer is defined as the portion of the boundary layer far enough from the surface to render molecular viscosity negligible relative to $\nu_{t,m}$, but close enough for convective effects to be negligible relative to the rate at which the turbulence is being created and destroyed (equilibrium turbulence state).

Notice that the Reynolds shear stress τ is constant in the wall layer and equal to the friction velocity (or shear velocity, u_τ) implying that $\tau/k=\sqrt{\beta^*_\infty}$ and leading to the standard value for β^*_∞ because a variety of experimental measurements [43] indicate that for simple shear flows the ratio of τ/k is about 3/10 in the wall layer. Thus, the predicted wall layer solution is consistent with experimental observations, providing this base value for β^*_∞ for simple shear flows.

4 Incipient Cavitation State Into the Nozzle Study

For the grid M03, an incipient cavitation state ($\sigma=1.19$, see Fig. 1) was first modeled using the default values for all the

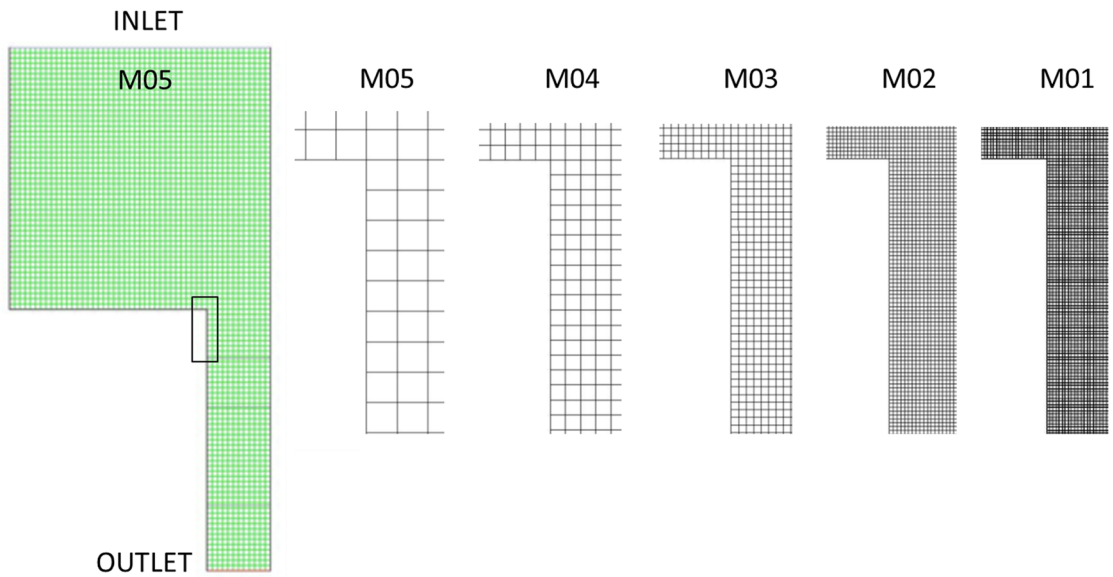

Fig. 3 Cells size comparison of the used meshes, see more details in Table 1

Table 2 CFD results (M03, $\sigma = 1.19$): mean velocity averaged at the outlet, $c_{m,\text{out}}$ (m/s)

Exp.	SA	Ske	RNG	SST ($\beta^* = 0.09$, default)	SST ($\beta^*_\infty = 0.11$)	SST ($\beta^* = 0.18$)
12.800	12.754	12.727	12.745	12.724	12.734	12.790
Error (%)	0.36	0.57	0.43	0.59	0.51	0.08

Note: The error for the used EVMs was computed taking as the exact value the measured one.

calibration parameters of the selected EVMs. Also, the RNG turbulence models [33] were added to study its performance under these incipient/developed cavitation conditions and to compare the obtained results against the ones from Ref. [9].

Second, this case was modeled by the SST model with a fine tuning of the β^*_∞. After that, comparisons between experiments and CFD simulations were performed for: (1) The averaged c_m at the outlet, i.e., $c_{m,\text{out}}$, Table 2. (2) Both c_m and c'_{RMS} profiles at positions y_1, y_2, y_3, Figs. 3 and 4. (3) The cavity shape (vapor fraction), Fig. 1 (and some details in Fig. 5).

Table 2 shows that all the used EVMs underpredict the $c_{m,\text{out}}$ when the default calibration values were used. The SA model gives the best result and conversely, the SST model gives the worst prediction. Under the fine tuning of β^*_∞, it was observed that the $c_{m,\text{out}}$ predictions are improved, but for $\beta^*_\infty > 0.12$, some oscillations in the computed $c_{m,\text{out}}$ appear, despite the improvement obtained. These instabilities could be provoked by the excessive turbulent viscosity suppression by means of the tuning coefficient. Figure 4 shows that the models SA, SST, and RNG give similar predictions for the c_m profiles at all the checked positions. At y_1 and y_2 positions, the Ske model overpredicts the c_m profile in the zones nearer the left wall of the nozzle ($x < 0$) and they are smoother than the ones predicted by the other EVMs. The comparison against LES results from Fig. 1 shows a similar quality for the c_m adjustments obtained here. On the other hand, the c'_{RMS} profiles were strongly underpredicted by the SA model at all the positions. At positions y_1 and y_2, the SST model gives the best fitting for the c'_{RMS} profiles. The Ske model overpredicts the c'_{RMS} profile when $x > 0$. At position y_3, the c'_{RMS} predictions are improved by the Ske model, but conversely the results from the SST and the RNG models worsen.

In order to check if calibration allows saving some CPU resources, comparisons were carried out against: (1) The results from Ref. [9] computed in selectively refined grids (-7.3×10^4 – 6.2×10^5 cells) using the RNG and SST models, Fig. 6. (2) The results from Refs. [7] and [9] computed by using the LES Smagorinsky and Vreman's SGS models, see Figs. 1 and 4. These LES results needed time steps of order O(10^{-8}s), about 7.0×10^5 cells

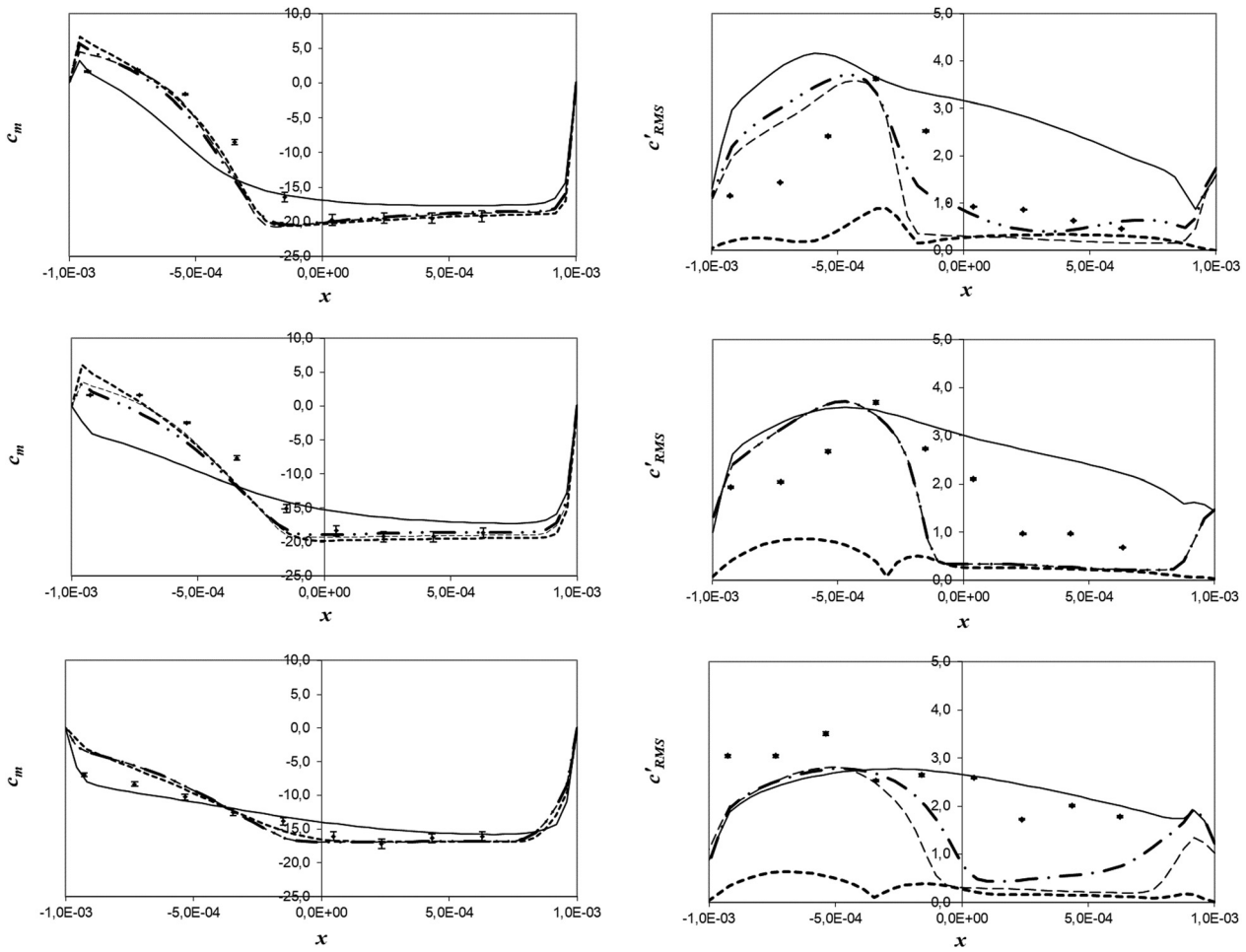

Fig. 4 CFD results (M03, $\sigma = 1.19$): Velocity profiles: c_m (left) and c'_{RMS} (right). Top: y_1, Middle: y_2, Bottom: y_3. x (mm), lateral coordinate (nozzle); ○, exp. [7,9], (vertical bars point out uncertainty); CFD: ----, SA; —, Ske; – – –, SST (β^*_∞ =0.09); – ·· –, RNG.

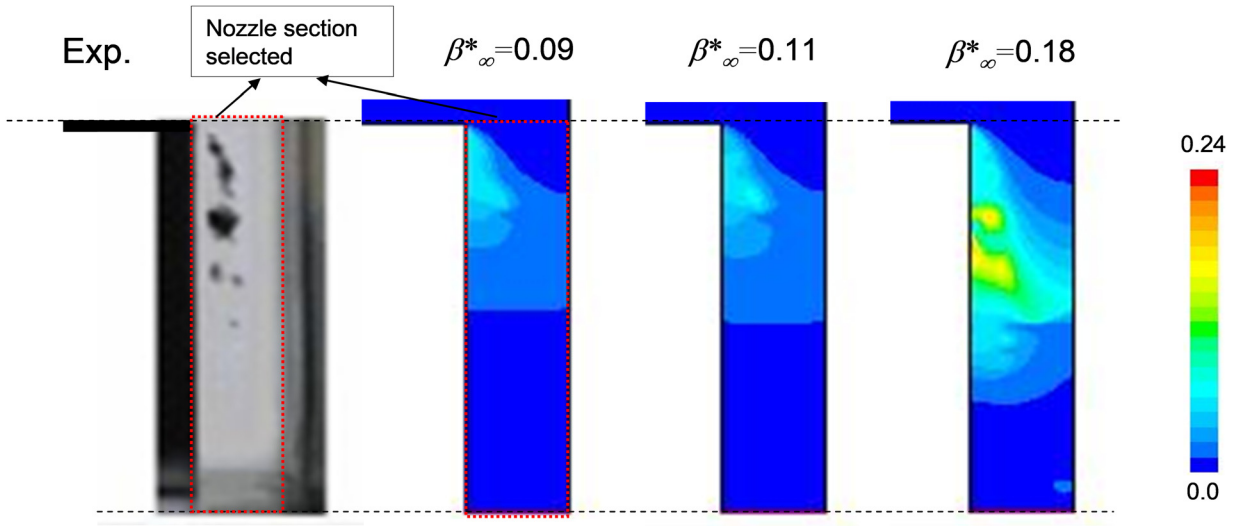

Fig. 5 CFD results (M03, $\sigma = 1.19$, β^*_∞ sensitivity study): cavity shape (vapor fraction). Exp., experiments [7]; Red/dotted frame, measurement/CFD domain; β^*_∞, calibration parameter, SST model.

for a precursor simulation to obtain a suitable inlet boundary condition and 2.8×10^6 cells in the nozzle simulations involving high CPU requirements (e.g., a Linux computer with 3.0 GHz × 32 core, 16 CPU, and 64 GB memories per node was used for the numerical calculations. The CPU time for a precursor simulation was about three weeks to reach a steady-state, while that for a nozzle simulation was about one week [7,9]).

Despite the coarser grid used, the comparison between the results from the RNG and SST models obtained in this work and the ones from Ref. [9] maintain similar quality, Fig. 6. The

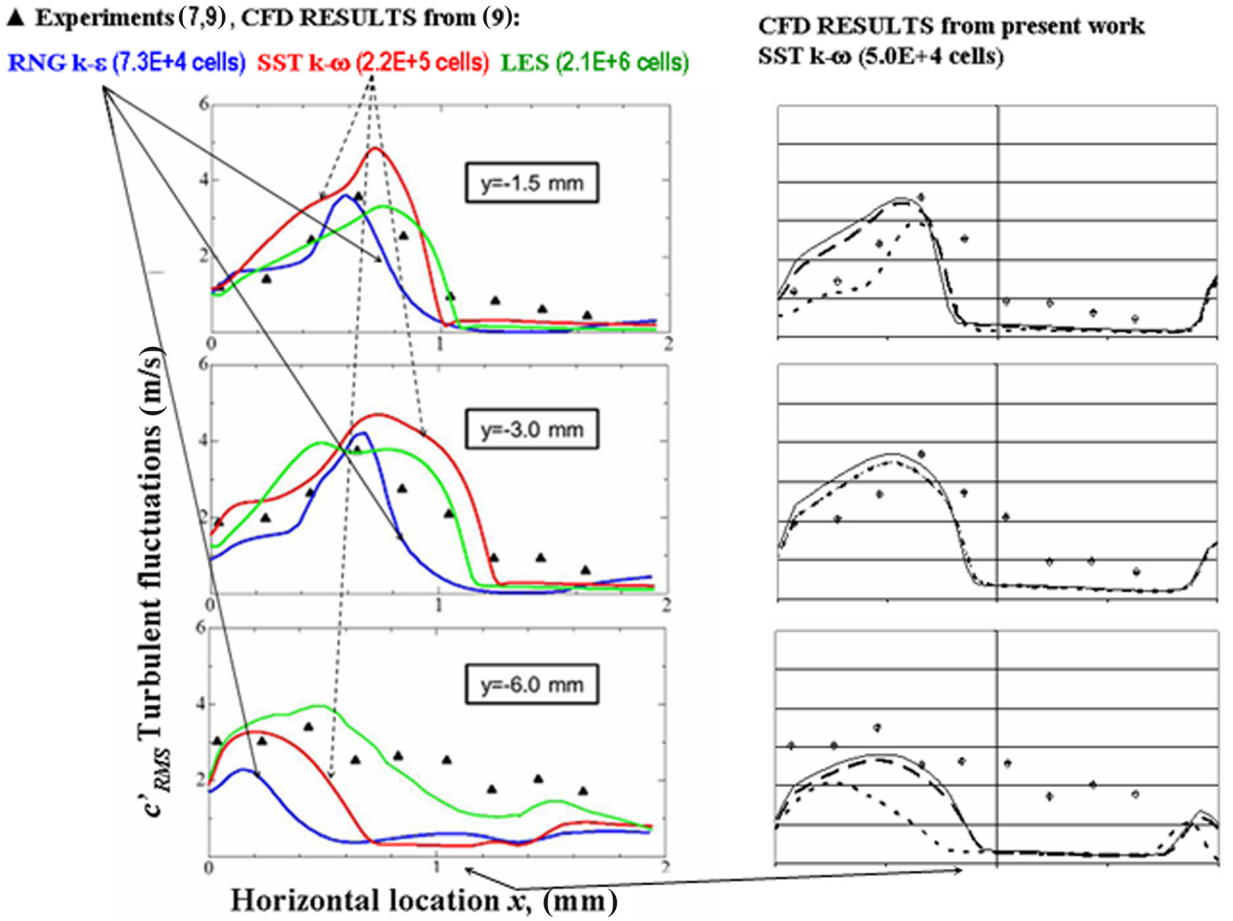

Fig. 6 CFD results (M03, $\sigma = 1.19$, β^*_∞ sensitivity study): fluctuating velocity profiles: c'_{RMS}. Left: CFD results from Ref. [9]. Right: CFD this work: ○, exp. [7,9], (vertical bars point out uncertainty); CFD: —, 0.09; – – –, 0.12; ---- , 0.18. For a clearer curves identification: Full arrows point RNG model, dotted arrows point SST model. Curves without arrows were obtained by LES modeling.

comparison between Figs. 1, 3, and 4 shows a similar quality for the predicted c_m profiles and a clear improvement of the c'_{RMS} profiles predicted at the incipient cavitation zone concluding that it is possible to obtain RAS/EVMs results of similar quality to the LES simulations, but saving a lot of CPU resources by means of the GCI+Richardson extrapolation study and a careful SST calibration. Despite the SST predictions worsened at the position y_3 compared with the LES ones, apparently the cavity formation is not affected so much. Figure 5 shows the general shape of the cavity predicted by the SST model when the calibration parameter β^*_∞ is changed. The red frame remarks the measurement zone/computational domain because the acrylic front wall introduces some distortions in the nozzle image in the experiments [8,9].

It is shown that depending on the selected value for $\beta^*_{\infty,}$ the μ_t is suppressed at position y_1 leading to a rise in the vapor fraction predicted. Therefore, the incipient/developed unsteady nature of cavitation at $\sigma = 1.19$ in this geometry is captured despite the steady-state simulation performed because: (1) The "incipient shedding" is better observed. (2) The $c_{m,out}$ prediction improves, Table 2. (3) The fluctuating velocity field, c'_{RMS}, at the nozzle inlet it is better adjusted for $\beta^*_\infty > 0.09$ values, Fig. 6.

Unfortunately, in the experiments, there is no quantitative information about the vapor fraction level and in the CFD simulations from Refs. [7] and [9] there are no images with the cavity shape for $\sigma = 1.19$. Therefore, only the cavity shape from experiments could be compared against the present CFD results, assuming that in the cavity shown by the experiments the vapor fraction values are not nearer the unity, since the fluid reached the incipient cavitation state only.

5 Conclusions

Several EVMs were used for modeling an incipient/developed cavitating flow state, $\sigma = 1.19$ in an asymmetrical inlet/square outlet section nozzle configuration after a careful GCI+Richardson extrapolation study and a careful EMVs calibration at $\sigma = 1.91$. The obtained results by using the M03 grid showed independence from the cell size and this grid was then used for the EVM calibration tasks. Also, a detailed calibration of the SST model allows improving both the cavity shape and the velocity field predictions in the zones downstream the nozzle edge (i.e., nozzle inlet, see Fig. 1).

It was demonstrated that the calibration task constitutes the first and necessary step to detect the incipient cavitation state accurately, improving the performance of the EVMs by calibration. At this stage, the results obtained are acceptable and competitive against the ones obtained by LES. The methodology for the calibration performed could be a general strategy in the sense that it was defined in terms of physical reasoning related to the differences in the flow structure when shear flows and detached flows are compared.

The improvements in the obtained results are justified in the fact that the coefficient β^*_∞, is responsible for the computed level in the dissipation of the turbulence kinetic energy (k) and the production of its dissipation (ω). The production of k depends of the main flow; instead, its dissipation depends on how the k is transported by turbulent convection. Therefore, the main characteristic of the geometry (i.e., the nozzle edge, see Fig. 1) is related to the k production, not to the k dissipation, being the last effectively related to β^*_∞.

At $\sigma = 1.19$, a steady-state simulation is still possible to compare "steady" experimental and CFD results for both mean and fluctuating velocity fields. It is demonstrated that the improvements in the fluctuating velocity field predictions provoke a more accurate cavity shape prediction. The mean velocity field c_m does not suffer strong variations when the calibration is performed, but the c'_{RMS} field predicted is strongly affected by the calibration. This fact remarks the close relation between the turbulence level and the cavitation inception phenomenon because it was demonstrated that suppressing the $\nu_{t,m}$ level by calibration the vapor fraction predicted rises.

A more detailed investigation will be necessary to explain why the results obtained do not reach the asymptotic range for ϕ_1 when the grid M01 is used. The NWM strategy activated by the CFD code could be responsible for this deficiency because the computed pressure fluctuations, which are correlated to the $\nu_{t,m}$ level predicted in zones nearer the nozzle inlet, could play a role of paramount importance in the cavity development, being necessary in a more accurate turbulence modeling. It becomes clear that the use of nonlocal parameters (i.e., mean velocities, discharge coefficient, or flow rate) would not be enough to obtain accurate predictions in cavitating flows, which are conducted by local fluctuations of pressure. It is necessary to check the wall pressures or other local measurements for accurate predictions too, despite these experimental measurements are not commonly available due to the strong difficulties to obtain them.

The promising SST model performance can lead to future applications when an available modified version of it (i.e., SST/SAS) related to unsteady turbulence modeling will be used. SST/SAS would allow studies of developed cavitating flows by means of an unsteady less expensive RAS simulation instead of the LES option because LES applications for simulating turbulent flows in complex geometries (industrial flows) are not completely affordable nowadays. The obtained results reinforce the strategies for an initial design of low-pressure injectors by fast and credible results by using RAS simulations. One of the goals of this work was to obtain competitive results using modest computational resources thinking in future applications over more complex injector's geometry or other devices working under cavitation conditions (e.g., hydraulic turbomachines). RAS simulations still could be competitive for unsteady state simulations if a careful compromise between very detailed results and CPU requirements is considered.

Acknowledgment

This current work was partially supported by the Universidad Tecnológica Nacional (UTN) within its own research programme (UTN/SCTyP). Authors would like to express their appreciation to the UTN for providing financial support for this study (research projects UTI3504TC, UTI3543TC, and UTI4905TC).

Funding Data

- Universidad Tecnológica Nacional (Grant Nos. UTI3504TC, UTI3543TC and UTI4905TC; Funder ID: 10.13039/100009483).

Nomenclature

Variables and Parameters

$c_{m,out}$ = outlet flow velocity (m/s)
c'_{RMS} = RMS fluctuating flow velocity (m/s)
c_σ = characteristic flow velocity scale (m/s)
c_1 = inlet flow velocity (m/s)
h = cell length (m)
k = turbulence specific kinetic energy (m^2/s^2)
L_σ = characteristic length scale (m)
$\dot{m}$ = mass flow (m^3/s)
N_h = number of cells along the left nozzle wall (N-d)
p_{in} = mean inlet pressure (Pa)
p_{out} = mean outlet pressure (Pa)
p_v = mean vapor pressure (Pa)
Re = Reynolds number (N-d)
Sr = Strouhal number (N-d)
t, t_σ = characteristic time of the unsteadiness (s)
th_{out} = outlet orifice/nozzle thickness (m)
$y+$ = nondimensional wall distance (N-d)

w_{out} = outlet orifice/nozzle width (m)
We = Weber number (N-d)

Greek Symbols

β^*_∞ = calibration coefficient in production/dissipation terms, SST k–ω model, (N-d)
ε = rate of dissipation of kinetic energy, (m^2/s^3)
ν = liquid (mixture) kinematic viscosity (m^2/s)
$\nu_{t,m}$ = liquid (mixture) turbulent kinematic viscosity (m^2/s)
ρ = liquid (mixture) density (kg/m^3)
σ = cavitation number (N-d)
$\tau_{w,i}$ = local wall stress (Pa)
ϕ_i = ad-hoc functions defined for the Richardson extrapolation
ω = specific dissipation rate of kinetic energy ($1/s^2$)

Special Symbols

$\sim$ = approximately (N-d)
$\sim$O() = order of… levels, errors, residuals (N-d)

Acronyms

CFD = computational fluid dynamics
CPU = central process unit
EVMs = eddy viscosity model(s)
GCI = grid convergence index
LDV = laser Doppler velocimeter
LES = large eddy simulation
NS = Navier Stokes equations
NWM = near-wall modeling strategy
PRESTO = pressure staggering option, (pressure interpolation scheme)
QUICK = quadratic upstream interpolation for convective kinematics (higher-order differencing scheme)
RAS = Reynolds averaged simulations
RMS = root-mean-square
RSM = Reynolds stress modeling model
SA = Spalart Allmaras turbulence model
SAS = scale adaptative simulation
SGS = subgrid scale
SIMPLE = semi-implicit method for pressure-linked equations (used for solving NS equations)
SIMPLEC = semi-implicit method for pressure linked equations-consistent (used for solving NS equations)
SST k–ε = shear stress transport k–ε model
Std k–ε = standard k–ε
TEM = transport equation-based modeling
TMF = turbulent multiphase flow modeling

References

[1] Knapp, R., Daily, J., and Hammit, F., 1970, *Cavitation*, McGraw-Hill, New York.
[2] Brennen, C., 1995, *Cavitation and Bubble Dynamics*, Oxford University Press, New York.
[3] Brennen, C., 2005, *Fundamentals of Multiphase Flows*, Cambridge University Press, Cambridge, UK.
[4] Li, H., Kelecy, F., Egelja-Maruszewski, A., and Vasquez, S., 2008, "Advanced Computational Modeling of Steady and Unsteady Cavitating Flows," ASME Paper No. IMECE2008-67450.
[5] Shi, J., and Arafin, M., 2010, "CFD Investigation of Fuel Property Effect on Cavitating Flow in Generic Nozzle Geometries," ILASS–Europe2010, 23rd Annual Conference on Liquid Atomization and Spray System, Czech Republic, Sept. 6–8, Paper No. 90.
[6] Zhang, H., Han, B., Yu, X. G., and Ju, D. Y., 2013, "Numerical and Experimental Studies of Cavitation Behavior in Water-Jet Cavitation Peening," Process. Shock Vib., **20**(5), pp. 895–905.
[7] Sou, A., Biçer, B., and Tomiyama, A., 2014, "Numerical Simulation of Incipient Cavitation Flow in a Nozzle of Fuel Injector," Comput. Fluids, **103**, pp. 42–48.
[8] Biçer, B., and Sou, A., 2014, "Numerical Simulation of Turbulent Cavitating Flow in Diesel Fuel Injector," Proceedings of the Third International Symposium of Maritime Science, Nov. 10–14, Japan, 3, pp 33–38.
[9] Biçer, B., 2015, "Numerical Simulation of Cavitation Phenomena inside Fuel Injector Nozzles," Ph.D. thesis, Kobe University, Japan.
[10] Bardow, A., Bischof, C. H., Martin Bücker, H., Dietze, G., Kneer, R., Leefken, A., Marquardt, W., Renz, U., and Slusanschi, E., 2008, "Sensitivity-Based Analysis of the k–ε Model for the Turbulent Flow Between Two Plates," Chem. Eng. Sci., **63**(19), pp. 4763–4775.
[11] Coussirat, M., Moll, F., Cappa, F., and Fontanals, A., 2016, "Study of Available Turbulence and Cavitation Models to Reproduce Flow Patterns in Confined Flows," ASME J. Fluids Eng., **138**(9), p. 091304.
[12] Coussirat, M., Moll, F., and Fontanals, A., 2017, "Reproduction of the Cavitating Flows Patterns in Several Nozzles Geometries Using Calibrated Turbulence and Cavitation Models," Mec. Comput., **XXXV**, pp. 819–841.
[13] Singhal, A., Athavale, M., Li, H., and Jiang, Y., 2002, "Mathematical Basis and Validation of Full Cavitation Model," ASME J. Fluids Eng., **124**(3), pp. 617–624.
[14] Schnerr, G., and Sauer, J., 2001, "Physical and Numerical Modeling of Unsteady Cavitation Dynamics," Fourth International Conference Multiphase Flow, New Orleans, LA, May 27–June 1.
[15] Coutier-Delgosha, O., Reboud, L. Y., and Delannoy, Y., 2003, "Numerical Simulation of the Unsteady Behaviour of Cavitating Flows," Int. J. Num. Meth. Fluids, **42**(5), pp. 527–548.
[16] Coussirat, M., Moll, F., and Fontanals, A., 2018, "Cavitating Flow Pattern Characterization in Square Section Injectors by Means of CFD," Mec. Comput., **XXXVI**, pp. 1163–1172.
[17] Sou, A., Hosokawa, S., and Tomiyama, A., 2007, "Effects of Cavitation in a Nozzle on Liquid Jet Atomization," Int. J. Heat Mass Transfer, **50**(17–18), pp. 3575–3582.
[18] Sou, A., Maulana, M., Hosokawa, S., and Tomiyama, A., 2008, "Ligament Formation Induced by Cavitation in a Cylindrical Nozzle," J. Fluid Sci. Technol., **3**(5), pp. 633–644.
[19] Sou, A., Maulana, M., Isozaki, K., Hosokawa, S., and Tomiyama, A., 2008, "Effects of Nozzle Geometry on Cavitation in Nozzles of Pressure Atomizers," J. Fluid Sci. Tech., **3**(5), pp. 622–632.
[20] Bicer, B., and Sou, A., 2015, "Numerical Models for Simulation of Cavitation in Diesel Injector Nozzles," Atomization Sprays, **25**(12), pp. 1063–1080.
[21] Koukouvinis, P., Naseri, H., and Gavaises, M., 2017, "Performance of Turbulence and Cavitation Models in Prediction of Incipient and Developed Cavitation," Int. J. Eng. Res., **18**(4), pp. 333–350.
[22] Biçer, B., and Sou, A., 2015, "Turbulence and Bubble Dynamics Models to Simulate Transient Cavitation Flow in Fuel Injector Nozzle," 13th Triennial International Conference on Liquid Atomization and Spray Systems (ICLASS 2015), Tainan, Taiwan, Aug. 23–27, pp. 1–8.
[23] Vashahi, F., Dafsari, R., Rezaei, S., Lee, J., and Baek, B., 2019, "Assessment of Steady VOF RANS Turbulence Models in Rendering the Internal Flow Structure of Pressure Swirl Nozzles," Fluid Dyn. Res., **51**(4), p. 045506.
[24] Edelbauer, W., Strucl, J., and Morozov, A., 2015, "Large Eddy Simulation of Cavitating Throttle Flow," Advances in Hydroinformatics, P. Gourbesville, J. Cunge, and G. Caignaert, eds., Springer Water, Srpinger, Singapore, pp. 501–517.
[25] Zwart, J., Gerber, A., and Belamri, T., 2004, "Two-Phase Flow Model for Predicting Cavitation Dynamics," Proceedings of Fifth International Conference on Multiphase Flow, Yokohama, Japan, Paper No. 152.
[26] Ali, M., Doolan, C., and Wheatley, V., 2009, "Convergence Study for a Two-Dimensional Simulation of Flow Around a Square Cylinder at a Low Reynolds Number," Seventh International Conference on CFD in the Minerals and Process Industries CSIRO, Australia.
[27] Celik, I., Ghia, U., Roache, P., Freitas, C., Coleman, H., and Raad, P., 2008, "Procedure for Estimation and Reporting of Uncertainty Due to Discretization in CFD Applications," ASME J. Fluids Eng., **130**(7), p. 078001.
[28] Roache, P., 1997, "Quantification of Uncertainty in Computational Fluid Dynamics," Annu. Rev. Fluid. Mech., **29**(1), pp. 123–160.
[29] Xing, T., and Stern, F., 2010, "Factors of Safety for Richardson Extrapolation," ASME J. Fluids Eng., **132**(6), p. 061403.
[30] Roache, P., 2011, "Discussion: Factors of Safety for Richardson Extrapolation (Xing T., and Stern F.2010, ASME J. Fluids Eng., 132, pp. 061403)," ASME J. Fluids Eng., **133**(11), p. 115501.
[31] Dular, M., and Bachert, R., 2009, "The Issue of Strouhal Number Definition in Cavitating Flow," J. Mech. Eng., **55**(11), pp. 666–674.
[32] Escaler, X., Egusquiza, E., Farhat, M., Avellan, F., and Coussirat, M., 2006, "Detection of Cavitation in Hydraulic Turbines," Mech. Syst. Signal Process., **20**(4), pp. 983–1007.
[33] Versteeg, H., and Malalasekera, W., 2007, *An Introduction to Computational Fluid Dynamics: The Finite Volume Method*, 2nd ed., Pearson Prentice Hall, Upper Saddle River, NJ, p. 503.
[34] Durbin, P., and Pettersson, R., 2011, *Statistical Theory and Modeling for Turbulent Flows*, 2nd ed., Wiley, Hoboken, NJ.
[35] Menter, F., 1994, "Two Equations Eddy-Viscosity Turbulence Models for Engineering Applications," AIAA J., **32**(8), pp. 1598–1605.
[36] Spalart, P., and Allmaras, R., 1994, "A One-Equation Turbulence Model for Aerodynamic Flows," Recherche Aerospatiale, No. 1, pp. 5–21.
[37] Wilcox, D., 1998, *Turbulence Modeling for CFD*, DCW Industries, La Cañada, CA.
[38] Ansys, "Ansys Fluent Software," Ansys, accessed Nov. 17, 2020, http://www.ansys.com/Industries/Academic/Tools/

[39] Menter, F., Kuntz, M., and Langtry, R., 2003, "Ten Years of Industrial Experience With the SST Turbulence Model," *Turbulence, Heat and Mass Transfer*, Begell House, pp. 625–632.
[40] Egorov, Y., Menter, F., Lechner, R., and Cokljat, D., 2010, "The Scale-Adaptive Simulation Method for Unsteady Turbulent Flow Predictions—Part 2: Application to Complex Flows," Flow Turbul. Combust., **85**(1), pp. 139–165.
[41] Menter, F., and Egorov, Y., 2010, "The Scale-Adaptive Simulation Method for Unsteady Turbulent Flow Predictions—Part 1: Theory and Model Description," Flow Turbul. Combust., **85**(1), pp. 113–138.
[42] Wilcox, D., 1988, "Reassessment of the Scale-Determining Equation for Advanced Turbulence Models," AIAA J., **26**(11), pp. 1299–1310.
[43] Townsend, A. A., 1976, *The Structure of Turbulent Shear Flow*, 2nd ed., Cambridge University Press, Cambridge, UK, pp. 107–108.